

Alteration of braunite ores from Eastern Liguria (Italy) during syntectonic veining processes: mineralogy and fluid inclusions

PIETRO MARESCOTTI¹ and MARIA LUCE FREZZOTTI²

¹Dipartimento per lo Studio del Territorio e delle sue Risorse, Università di Genova,
16132 Genova, Italy. – e-mail: marescot@dipteris.unige.it

²Dipartimento di Scienze della Terra, Università di Siena, 53100 Siena, Italy
E-mail: frezzotti@dst.unisi.it

Abstract: The manganese ores of the Northern Apennine ophiolites (Val Gravegila, Eastern Liguria, Italy) occur within chert sequences, mainly as stratiform layers (0.1–1 m thick) or massive lenses (5–20 m thick). The ores originated in the Ligurian-Piedmont oceanic basin (Middle Callovian) during turbiditic resedimentation of hydrothermally Mn-enriched submarine muds. During Upper Cretaceous–Lower Cenozoic orogenic events, the primary sedimentary oxide assemblages were completely recrystallized to braunite + quartz assemblages under prehnite-pumpellyite facies conditions ($T = 275 \pm 25^\circ\text{C}$; $P = 2.5 \pm 0.5$ kbar). This tectonic event induced mobilisation of Mn and Si, and thickening of the mineralised layers. A complex network of sigmoidal quartz veins formed at this stage. The interaction between the Mn mineralisation and the circulating fluids generated centimetric to decimetric reaction rims in the wall rock, where the braunite + quartz assemblage is replaced by Mn silicates (mainly bementite, johannsenite, parsettsenite and rhodonite) and carbonates (mainly Mn-bearing calcite and rhodochrosite) with a zoned distribution. Mineral zoning points to an early interaction between the Mn mineralisation and $\text{H}_2\text{O}-\text{CO}_2$ fluids with high water activity. Two distinct types of fluids are present in syntectonic quartz veins, namely a low-salinity water-rich fluid, and a Mn-Ca-Na-Mg-Fe-bearing aqueous solution that in all probability represent a relict of an early fluid phase circulating during breakdown of braunite. The isochore distribution related to low-salinity fluids indicates that veining processes took place during the main tectono-metamorphic events, at peak P-T conditions.

Key-words: Liguria, manganese ore, braunite, fluid inclusions, metamorphic fluids.

Introduction

Braunite + quartz is the most common assemblage in metamorphosed, sedimentary-diagenetic, and hydrothermal manganese ores (Roy, 1980, 1981; Dasgupta & Manickavasagam, 1981; Ostwald, 1992). In metamorphic deposits, braunite + quartz has been reported as the stable assemblage over a wide range of metamorphic conditions, spanning from chlorite to sillimanite grade (Bhattacharyya *et al.*, 1984). However, in natural systems, many questions remain unanswered especially regarding their stability as a function of the variation of chemical factors.

In the northern Apennine Mn ores braunite + quartz represent the stable mineral assemblage during the entire tectono-metamorphic evolution, up to prehnite-pumpellyite-facies conditions ($T = 275 \pm 25^\circ\text{C}$; $P = 2.5 \pm 0.5$ kbar; Lucchetti *et al.*, 1990). During metamorphism, however, the development of syntectonic fracture systems provided preferential pathways for extensive fluid circulation within the manganese ores and triggered the breakdown of the braunite + quartz assemblage, as a consequence of the variation of the chemical conditions.

The aim of this study is to evaluate the mechanism and the physicochemical constraints of the

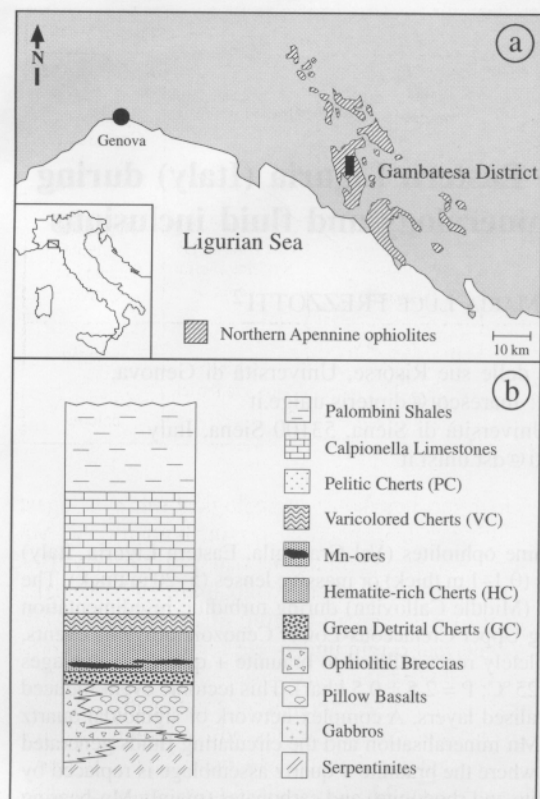


Fig. 1. a) Locality map of Gambatesa District and Northern Apennine Ophiolites (modified from Cabella *et al.*, 1998); b) stratigraphic sequence of Northern Apennine ophiolites and sedimentary covers in the Gambatesa District area (modified from Cabella *et al.*, 1994).

breakdown processes in the Northern Apennine Mn ores by means of textural, mineralogical and fluid-inclusion studies.

Geological setting

The manganese ore deposits of the "Gambatesa District", named after the largest mine in the district, are located in Eastern Liguria, over an area of almost 50 km², between the Graveglia and Bargonasco valleys (Fig. 1a). In the district 13 different ore deposits have been mined from 1885 to 1990, and in this period about 1.200.000 tons of Mn-ore minerals were extracted. Ores occur within cherts of the Diaspri di Monte Alpe Formation, close to the contacts with the underlying Jurassic ophiolites of the Northern Apennines (Cortesogno *et al.*, 1979; Cabella *et al.*, 1994, 1998).

The Northern Apennine ophiolites represent slices of the Jurassic Ligurian-Piedmont oceanic crust separating paleo-European and Adria continental blocks. They consist of ultramafic and/or gabbroic basement, overlain by a volcano-sedimentary sequence, represented, from bottom to top, by tectonic and sedimentary breccias, massive and pillow basalts, cherts, calcareous shales and limestones (Fig. 1b); Cortesogno *et al.*, 1987; Principi *et al.*, 1992; Cabella *et al.*, 1994; Marescotti & Cabella, 1996). Both mafic and ultramafic rocks record two main cycles of ocean-floor metamorphic events, which also affected in part the overlying breccias and basalts; the metamorphic conditions evolved from high-T amphibolite facies to low-T hydrothermal conditions (Cortesogno & Lucchetti, 1984). During Late Cretaceous-Early Cenozoic orogenic events, the ophiolitic sequences and their sedimentary covers were affected by a tectono-metamorphic overprint that, in the mining area, reached a peak at prehnite-pumellyte facies conditions ($T = 275 \pm 25^\circ\text{C}$; $P = 2.5 \pm 0.5$ kbar; Lucchetti *et al.*, 1990).

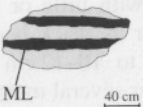
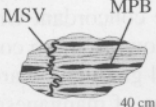

Analytical method

Identification of mineral species was achieved by means of microscopic examination (transmitted and reflected light), and X-ray diffraction analyses (XRD) on concentrated powder using a Siemens Cristaloflex IV diffractometer (Dipartimento per lo Studio del Territorio e delle sue Risorse, University of Genova). Powders were concentrated by repeated cycles of crushing, sieving and hand-picking as well as through magnetic methods. Instrument settings for XRD were: radiation, CuK α ; K β -filter, Ni; internal standard, NaF; generator tension, 30 kV; generator current, 22 mA; scan speed, $1^\circ 2\theta/\text{min}$; scan interval, $2.5\text{--}70^\circ 2\theta$.

The chemical composition of manganese minerals was determined using a WDS-ARL-SEMQ electron microprobe (Dipartimento di Science della Terra, University of Modena) operating at 15 kV accelerating voltage, 15 nA beam current, and with a beam spot diameter of about 3–4 μm . The following "SPI 53" international reference standards were used: albite, apatite, barite, calcite, celestite, diopside, dolomite, hematite, olivine, rhodonite, rutile, and sanidine. Moreover synthetic MnO₂ (99.9% Aldrich certified) was used to check the manganese oxides.

Fluid-inclusion studies were performed on doubly polished thin sections ($\sim 100 \mu\text{m}$) on a Lin-

Fig. 2. Sketch illustrating the polyphasic evolution, texture and mineralogy of manganese mineralization in Eastern Liguria. Abbreviations: ML, Graded-bedding mineralisation; MSV, mineralisation in syndiagenetic veins; MPB, mineralisation in pseudoboudins; MB, massive mineralisation in syntectonic boudins; MM, massive mineralisation in syntectonic lenses.

SETTING	EVENT	TYPE	TEXTURE	MINERALOGY
Ocean	Hydrothermal enrichment and resedimentation		Graded bedding	Amorphous Mn oxides and hydroxides Chalcedony Quartz
Ocean	Diagenesis		Graded bedding Pseudoboudins Syndiagenetic veins	Pyrolusite Braunite Chalcedony Quartz
Accretionary wedge	Orogeny		Boudins Massive lenses	Braunite Quartz Mn-bearing calcite

kam THMS-600 heating-freezing stage mounted on a Leitz Laborlux binocular microscope (Dipartimento di Scienze della Terra, University of Siena). Measurements were calibrated using synthetic and natural fluid-inclusion standards with phase transitions at -142°C (C_6H_{12}), -56.6°C (CO_2), 0°C (H_2O), 68°C ($\text{C}_6\text{H}_5\text{NO}$), and 199.8°C ($\text{CH}_3\text{C}_6\text{H}_4\text{NH}_2$). The heating and freezing rate of $5^{\circ}\text{C min}^{-1}$ was reduced to $1^{\circ}\text{C min}^{-1}$ on approaching the phase transitions to ensure thermal equilibration. Accuracy is $\pm 0.1^{\circ}\text{C}$ at the standard reference points.

Laboratory data were processed with the MacFlinco software (Brown & Hagemann, 1994). Isochores were calculated using the equation by Zhang & Frantz (1987).

In order to obtain more detailed information on the chemical composition of the fluid inclusions, selected wafers were broken and prepared according to the methods described in Shepherd *et al.* (1985). Precipitated salts were analyzed in opened inclusions by EDS on a SEM-Jeol Ltd. JSM-6400 (Faculty of Earth Sciences, Vrije Universiteit of Amsterdam). Operating conditions were 15 kV accelerating voltage, 20 nA beam current with a beam spot diameter of about 3–4 μm .

Qualitative and semi-quantitative gas-phase microanalyses were conducted of selected fluid inclusions with a Dilor Microdil-28[®] multichannel laser Raman microprobe (Faculty of Earth Sciences, Vrije Universiteit of Amsterdam; Burke, 1994).

Manganese ores of the Gambatesa District

The Mn ores of the Gambatesa District have undergone a complex polyphasic evolution (Fig. 2).

Their geochemistry and geological setting suggest a primary hydrothermal origin, both for the Mn ores and the adjoining hematite-rich cherts (Bonatti *et al.*, 1977; Cortesogno *et al.*, 1979; Cabella *et al.*, 1998). Mn-Fe-bearing siliceous muds of hydrothermal origin underwent resedimentation processes during the active extensional tectonics that caused a further gravitative fractionation of Mn oxides and Mn hydroxides, and, consequently, the genesis of the layered Mn ores. The gravitative origin of the Mn-mineralised layer is suggested by well-preserved textures such as size gradation of the detrital and biological (radiolarian tests) constituents, compositional gradation (*i.e.*, progressive decrease of the Mn/Si ratio from the base to the top of each mineralized layer), and parallel and convoluted laminations (Cortesogno *et al.*, 1979; Marescotti & Cabella, 1996).

As a consequence of diagenesis, the Mn-mineralised layers underwent mobilisation, compaction and recrystallisation processes; a first generation of braunite (occurring as a relict in syndiagenetic veins) is possibly related to this stage.

During Upper Cretaceous-Lower Cenozoic orogenic events the layered ores were affected by recrystallisation, mobilisation and thickening in areas of intense deformation and folding. Sedimentary-diagenetic Mn oxides and Mn hydroxides were completely replaced by the braunite + quartz assemblage under prehnite-pumpellyite-facies conditions (Lucchetti *et al.*, 1990).

At present, manganese ores in the Gambatesa District occur as massive lenses and boudins (MM and MB) but also as undeformed graded beds (ML). Mineralised syndiagenetic veins and pseu-

doboudins are occasionally preserved as relicts (Fig. 2).

ML are found in zones with little or no tectonic disturbance; they occur as black beds with metallic luster (from 3 mm to 10–12 cm thick), rhythmically interlayered over several metres with hematite-rich chert strata (up to 60 cm thick). Single mineralised layers are concordant with the enclosing cherts, typically showing sharp contacts at the base and compositional grading towards the top (e.g., progressive decrease of manganese content). The primary mineralogy, probably represented by poorly crystalline oxides and hydroxides (corresponding to the mineralogy of recent ocean-floor manganese deposits; Roy, 1980, 1981 and references therein; Usui & Someya 1997) is completely replaced by an intimate association of finely crystalline to massive anhedral braunite ($\text{Mn}^{2+}, \text{Ca}, \text{Mg})_{1-2x} (\text{Mn}^{3+}, \text{Al}, \text{Fe}^{3+})_{6+2x} \text{Si}_{1-2x} \text{O}_{12}$ (Abs-Wurnbach, 1980) and cryptocrystalline quartz with the braunite/(braunite + quartz) ratio varying from 0.7 to 0.5.

Both MM and MB mainly occur within mesoscopic chevron folds, respectively as plurimetric lens-shaped bodies (up to 50 m long and 30 m thick) and decimetre- to metre-sized boudins; massive lenses are located at the fold hinges whereas boudins occur along both fold limbs (Fig. 2). These ore types are characterised by euhedral to subhedral braunite associated with minor quartz and the braunite/(braunite + quartz) ratio varies from 0.8 to 0.7. Pyrolusite is widespread as oxidation product, either replacing braunite, or as dendritic films that coat open fissures.

At least three generations of braunite (braunite 1, 2 and 3) have been distinguished in ML, MM, and MB types of ores on the basis of textural evidence. Braunite 1 occurs mainly in the ML type and represents the first generation of braunite, growing at the expense of "primary" oxides and hydroxides; major evidence is in the colloform textures where microcrystals of braunite pseudomorphically replace the primary phases. Braunite 2 is found as coarse-grained, anhedral aggregates in massively textured ores, whereas braunite 3 commonly appears as blocky aggregates of euhedral crystals, associated with quartz and minor calcite. Braunite 2 and 3 represent products of metamorphic recrystallisation of braunite 1 and they are indistinguishable on the basis of their chemical composition.

Metasomatic minerals

A wide variety of metasomatic manganese minerals has been recognised in veins, and in the adjoining selvages, that cross-cut the massive ores (mainly MM). Three main groups can be distinguished; 1) Mn phyllosilicates (bementite and parsettensite), 2) Mn pyroxene and Mn pyroxenoid (johannsenite and rhodonite), and 3) Mn carbonates (Mn-bearing calcite, rhodochrosite, and possibly kutnahorite).

In the following paragraphs we give short descriptions of the occurrence and textural and chemical features of these minerals.

1) *Mn phyllosilicates (bementite and parsettensite)*

Bementite, $\text{Mn}_7\text{Si}_6\text{O}_{15}(\text{OH})_8$ (Heinrich *et al.*, 1994), is present as brownish-orange cryptocrystalline massive aggregates and, less common, as light brown-pinkish fibrous-lamellar flakes, often intergrown with carbonates. The chemical composition is quite uniform, with minor variations not related to different textural characters.

Parsettensite, $(\text{K}, \text{Na}, \text{Ca})_{7.5} (\text{Mn}, \text{Mg})_{49} (\text{Si}, \text{Al})_{72} \text{O}_{168} (\text{OH})_{50} \cdot n\text{H}_2\text{O}$ (Eggleton & Guggenheim, 1994), was identified by XRD patterns in light-brown clay-sized material. It always occurs as fibrous aggregates intimately intergrown with bementite. Due to these intimate intergrowths, quantitative chemical analyses of parsettensite could not be obtained.

2) *Mn pyroxene and Mn pyroxenoid (johannsenite and rhodonite)*

Johannsenite mainly occurs as pale gree-yellowish relicts of lamellar crystals, partially to almost completely replaced by rhodonite lamellae or by an assemblage of calcite + rhodonite + quartz. All the analysed johannsenite relicts approach the stoichiometric formula of $\text{CaMnSi}_2\text{O}_6$.

Rhodonite appears as a product of braunite, bementite, and johannsenite breakdown, and is often associated with Mn-bearing calcite and/or rhodochrosite. It occurs as colourless to light-pinkish aggregates of subhedral to euhedral crystals or as thin lamellae within johannsenite crystals. Variations of MnSiO_3 - CaSiO_3 mole% are common, and they are clearly related to different mineral assemblages (Fig. 3a and Table 1), as

Table 1. Representative microprobe analyses of rhodonite from reaction rims.

Reaction #	V	V	V	VI	VI	VI	II	II	II
wt%									
SiO ₂	46.51	47.06	45.65	47.14	46.10	46.46	47.15	45.78	47.10
TiO ₂	0.11	0.04	0.00	0.06	0.00	0.01	0.04	0.00	0.04
MnO	48.41	48.46	49.14	47.68	48.44	48.43	46.59	47.21	46.32
CaO	4.13	4.07	4.00	4.95	4.60	4.93	5.51	6.27	5.93
K ₂ O	0.04	0.04	0.00	0.03	0.00	0.00	0.04	0.00	0.03
Total	99.20	99.67	98.79	99.86	99.14	99.83	99.33	99.26	99.42
Number of cations on the basis of 3 oxygens									
Si	1.006	1.011	0.998	1.010	1.001	1.000	1.012	0.993	1.010
Ti	0.002	0.001	0.000	0.001	0.000	0.001	0.001	0.000	0.001
Mn	0.887	0.882	0.910	0.865	0.891	0.883	0.847	0.867	0.842
Ca	0.096	0.094	0.094	0.114	0.107	0.114	0.127	0.146	0.136
K	0.001	0.001	0.000	0.001	0.000	0.000	0.001	0.000	0.001
Total	1.992	1.989	2.002	1.991	1.999	1.998	1.988	2.006	1.990
MnSiO ₃	90.23	90.37	90.64	88.36	89.28	88.57	86.96	85.59	86.09
CaSiO ₃	9.77	9.63	9.36	11.64	10.72	11.43	13.04	14.41	13.91

Reaction number as described in text and depicted in Fig. 3 and 5.

CaSiO₃ content progressively decrease from the carbonate-free to the carbonate-bearing assemblages, and in the latter from rhodochrosite-bearing to manganiferous-calcite-bearing assemblages.

3) Carbonates

Analysed carbonates invariably represent virtually pure MnCO₃-CaCO₃ solid solutions. On the basis of MnCO₃/CaCO₃ ratios three different carbonate groups can be distinguished (Fig. 3b and Table 2).

1) CaCO₃-rich carbonate (Mn-bearing calcite) occurs as anhedral to subhedral crystals intimately associated with rhodonite, or as anhedral to fibrous crystals within veins along with bementite and/or rhodonite.

2) MnCO₃-rich carbonate (rhodochrosite) occurs as anhedral crystals associated with rhodonite or as fibrous-radiating aggregates within veins. The compositional gap between rhodochrosite and Mn-bearing calcite agrees well with the solubility gap defined by synthetic and natural low-grade metamorphic Mn and Ca carbonates ($T < 400^{\circ}\text{C}$; Goldsmith & Graf, 1957; Peacor *et al.*, 1987).

3) A third group occupies an intermediate field between group 1 and 2 carbonates, and has MnCO₃/CaCO₃ ratios between 0.4 and 0.6 (Fig. 3b and Table 2). Carbonates of this group are present in veins as minor constituents and mainly occur as

aggregates of fibrous crystals. Their compositions are very close to that of stoichiometric kutnahorite but no reflections suggesting dolomite-type carbonates have been detected in XRD patterns. Carbonates with this composition are not optically distinguishable, and they possibly represent intimate mixtures of two carbonates, one Ca-, the other Mn-rich. These compositions could alternatively be explained with a disordered phase such as "pseudokutnahorite" (Capobianco & Navrotsky, 1987) or "disordered kutnahorite" (Peacor *et al.*, 1987).

Syntectonic vein system

A complex network of syntectonic veins and joints often cross-cuts massive lens-shaped ore bodies present at fold hinges. These veins cross-cut the Mn ores with a direction parallel to the axial plane of the folds and are mainly located at the contacts between cherts and mineralized ore bodies. In some cases a syntectonic breccia, consisting of angular braunite + quartz clasts, set within a quartz \pm carbonates \pm Mn-silicates cement, developed as a consequence of volume expansion in the hinge zone of the chevron folds.

Most veins (0.5–2 cm wide) display composite textures and mineral infillings (Fig. 4a, b) with a

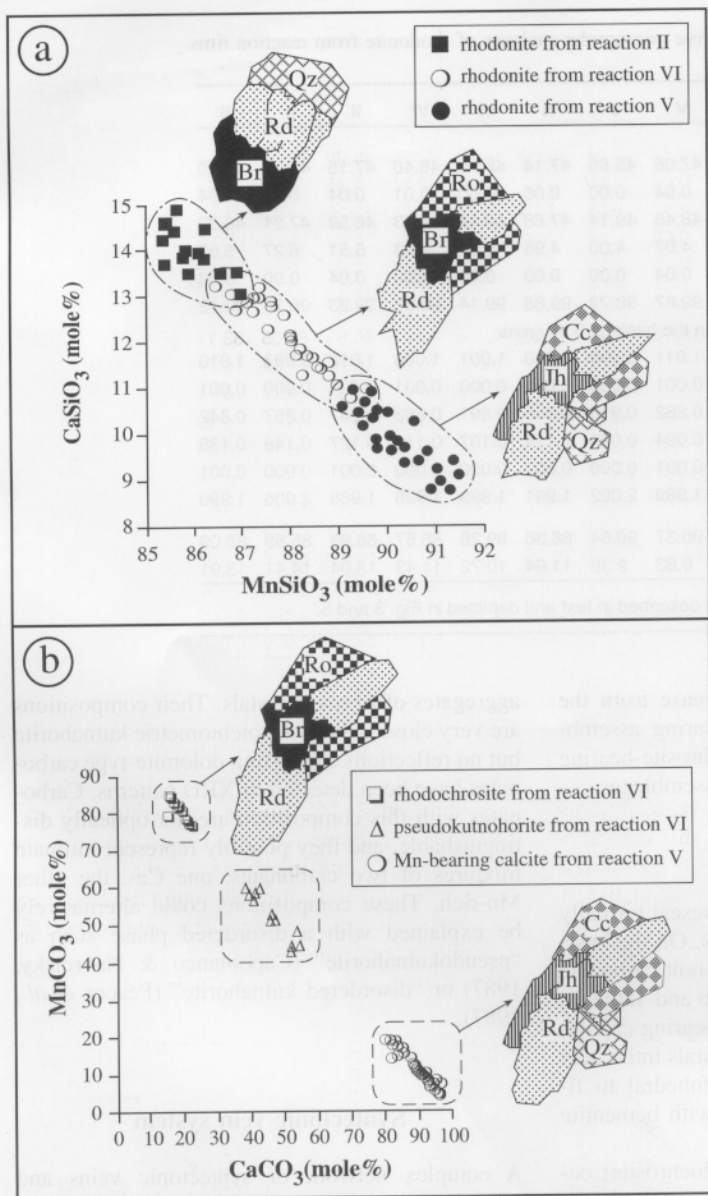


Fig. 3. a) Compositional variations of rhodonite from the different mineralogical assemblages; b) compositional variations of carbonates from the different mineralogical assemblages. Abbreviations, symbols and depicted reactions as in Fig. 5.

quartz-rich core (1) and two symmetric Mn-silicates + Mn-carbonate polycrystalline rims (2).

1) The vein core is mostly filled with quartz crystals of which the morphology varies from fibrous to columnar and blocky, often in the same vein. Transition between the different quartz textures occurs laterally, with the blocky quartz commonly located in curved and/or narrow sections of the vein. Fibrous and columnar quartz crystals (Fig. 4a) are elongated perpendicularly to the vein selvages; commonly one or more lines of braunite

inclusions are enclosed in the quartz fibres and run parallel to the vein selvages.

2) The polycrystalline rims display fibrous to fibrous-radiating textures and mainly consist of bementite, parsettensite and rhodonite intimately intergrown with Mn-bearing calcite and rhodochrosite. Transition between domains (1) and (2) is marked by fine-scale intergrowths of quartz, Mn carbonates and Mn silicates.

Centimetre- to decimetre-wide reaction rims are always present at the contacts between veins

Table 2. Representative microprobe analyses of carbonates from reaction rims.

Reaction #	V	V	V	VI	VI	VI	VI	VI	VI
wt%									
MnO	5.95	6.45	5.68	35.92	34.93	32.35	49.60	50.42	51.46
MgO	0.06	0.00	0.06	0.25	0.22	0.19	0.15	0.08	0.09
CaO	50.79	49.81	50.68	23.15	24.21	26.25	10.56	9.83	9.35
BaO	0.00	0.00	0.00	0.10	0.43	0.00	0.05	0.05	0.00
SrO	0.09	0.12	0.03	0.04	0.00	0.11	0.09	0.07	0.00
Total	56.89	56.38	56.45	59.46	59.79	58.90	60.45	60.45	60.90
MnCO _{3n}	9.59	10.50	9.22	58.07	56.14	52.51	80.59	82.05	83.17
CaCO _{3n}	90.16	89.33	90.61	41.22	42.86	46.93	18.90	17.62	16.64
MgCO _{3n}	0.13	0.00	0.13	0.52	0.46	0.40	0.32	0.17	0.19
BaCO _{3n}	0.00	0.00	0.00	0.13	0.55	0.00	0.07	0.07	0.00
SrCO _{3n}	0.13	0.17	0.04	0.06	0.00	0.16	0.13	0.10	0.00
Number of cations on the basis of 6 oxygens									
Mn	0.169	0.186	0.162	1.093	1.056	0.981	1.567	1.599	1.622
Ca	1.826	1.812	1.834	0.891	0.926	1.007	0.422	0.394	0.373
Mg	0.003	0.000	0.003	0.013	0.012	0.010	0.008	0.004	0.005
Ba	0.000	0.000	0.000	0.001	0.006	0.000	0.001	0.001	0.000
Sr	0.002	0.002	0.001	0.001	0.000	0.002	0.002	0.002	0.000
Total	2.000	2.000	2.000	1.999	2.000	2.000	2.000	2.000	2.000

XCO_{3n} = carbonate analyses normalized to 100%.

Reaction number as described in text and depicted in Fig. 3 and 5.

and massive manganese ores (Fig. 4a, b). The reaction rims commonly display distinct mineralogical zoning (Fig. 5). On the basis of mineral paragenesis, three zones can be distinguished. These are, from the unaltered braunite + quartz mineralisation towards the vein selvages: zone A) hydrous Mn-silicate zone (bementite and parset-

tensite); zone B) Mn-silicate zone (rhodonite and johannsenite); zone C) Mn-Ca-carbonate zone (Mn-bearing calcite and rhodochrosite).

In zone A bementite and minor rhodonite are the main reaction products; bementite is the first phase to form via the reaction:

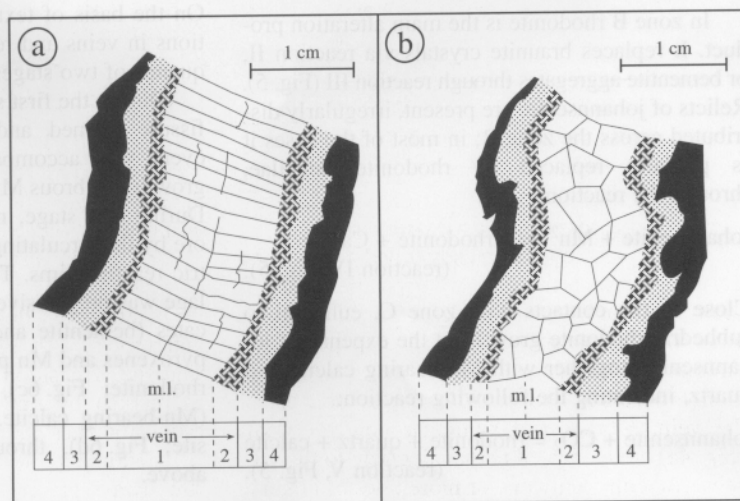


Fig. 4. Syntectonic fibrous (a) and blocky (b) composite veins. Symbols: 1) quartz core of the vein; 2) polycrystalline vein rims; 3) reaction zones; 4) massive mineralisations; m.l. = median line of the vein.

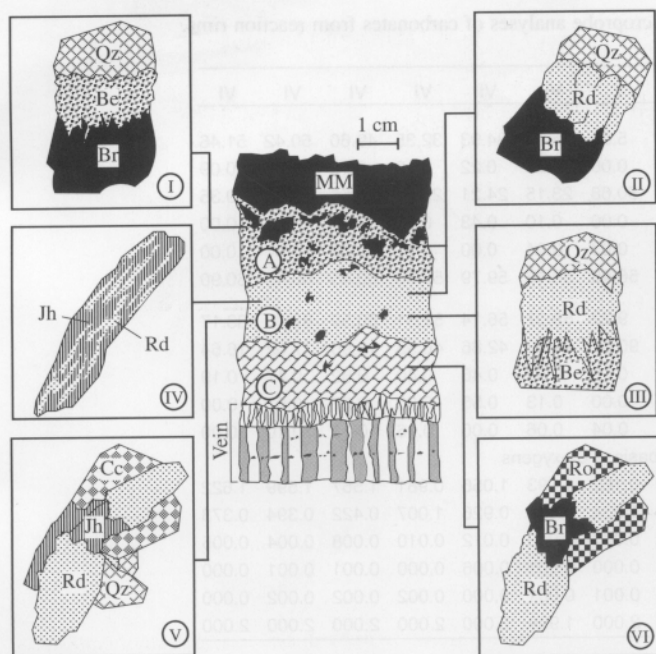
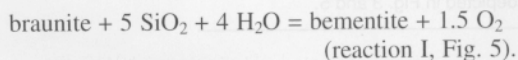
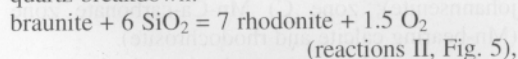


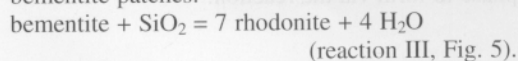
Fig. 5. Zonation of a reaction rim (zones A, B, and C as described in the text). Squares I, II, III, IV, V, and VI: schematic sketch of the observed reactions (as described in the text). Abbreviations: Be = bementite; Br = braunite; Cc = calcite; Jh = johannsenite; Qz = quartz; Ro = rhodochrosite; Rd = rhodonite; MM = massive mineralisation.



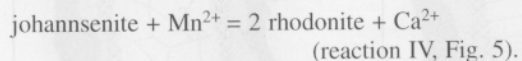
Rhodonite directly forms from the braunite + quartz breakdown:



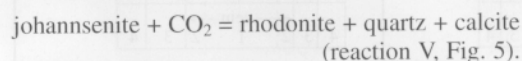
or, close to the contacts with zone B, it replaces bementite patches:



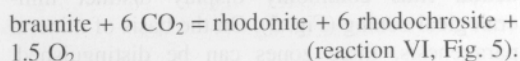
In zone B rhodonite is the main alteration product. It replaces braunite crystals via reaction II, or bementite aggregates through reaction III (Fig. 5). Relicts of johannsenite are present, irregularly distributed across the zone B; in most of the cases it is partially replaced by rhodonite lamellae, through the reaction:



Close to the contacts with zone C, euhedral to subhedral rhodonite growths at the expense of johannsenite, together with Mn-bearing calcite and quartz, indicating the following reaction:



In zone C, carbonates become the dominant alteration products; they are present in irregular patches or as intergrowth with rhodonite, replacing scattered braunite fragments:



Veining processes

On the basis of textural and mineralogical variations in veins and reaction rims we propose a sequence of two stages for the veining processes.

During the first stage (Fig. 6a–d) an extension fissure formed and propagated sideways: this event was accompanied by dynamic syntaxial growth of fibrous Mn silicates and Mn carbonates. During this stage, metasomatic alteration of Mn ore by the circulating fluid generated two symmetric reaction rims. The braunite + quartz assemblage was progressively replaced by Mn phyllosilicates (bementite and parsetensite; Fig. 6b), Mn pyroxenes and Mn pyroxenoids (johannsenite and rhodonite; Fig. 6c), and finally by carbonates (Mn-bearing calcite, kutnahorite and rhodochrosite; Fig. 6d), through the reactions described above.

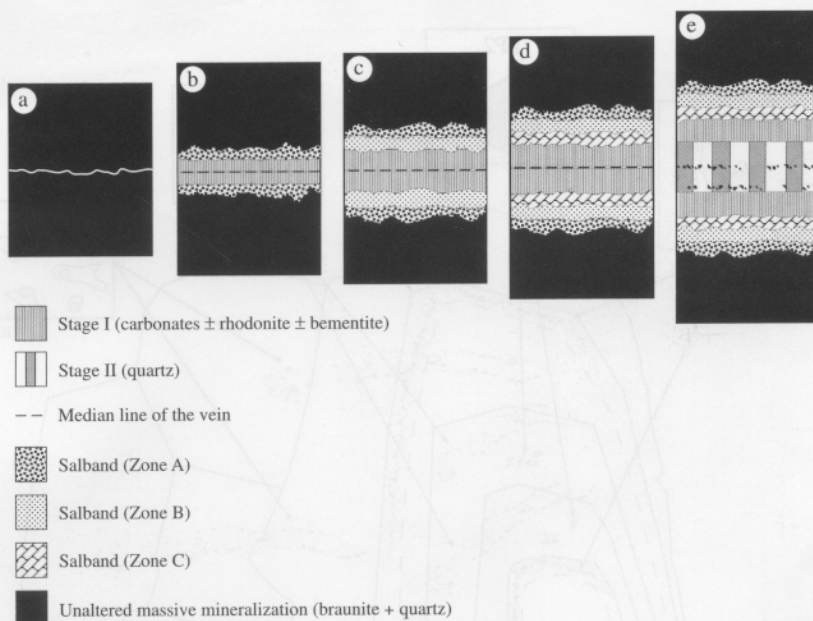


Fig. 6. Sketch of the hypothetical evolution of the syntectonic composite veins. a–d: syntaxial growth of carbonates \pm rhodonite \pm bementite and progressive development of the reaction rims; e: monomineralic quartz growth.

At the beginning of the second stage the fluid chemistry was presumably compatible with the generation of fibrous intergrowths of quartz + Mn carbonates + Mn silicates. Silica enrichment in the residual fluid caused late-stage precipitation of monomineralic quartz infillings (Fig. 6e).

In the quartz domain of the vein, the lateral changes from fibrous to blocky textures, occurring within curved and/or narrow sections of some veins, are probably related to local variations in the nucleation rates, producing differences in initial grain size (Urai *et al.*, 1991). Alternatively they can be related to occlusion during competitive fibre growth as described by Cox & Etheridge (1983), Ramsay & Huber (1983), and Cox (1987).

Fluid-inclusion studies

Petrography

In order to characterise the fluids circulating during the veining processes, we have analysed fluid inclusions in quartz crystals of the syntectonic veins.

The fibrous and the columnar quartz crystals are generally affected by retrograde deformation, shown by subgrain recrystallisation, undulatory extinction, and microfracturing. For the fluid-in-

clusion study, nine undeformed euhedral quartz grains, with well-defined growth zones (Fig. 7), were selected from six different vein samples. Four of these quartz crystals were located along the median line of the veins, the other five close to the contacts with the Mn silicates + Mn carbonates domain of the veins, where they clearly show intergrowth relationships with rhodonite and/or carbonates.

Fluid-inclusion investigations in carbonate minerals were unsuccessful, as these decrepitated during the heating cycle.

All studied fluid inclusions contain two phases (Liquid + Vapour) at room temperature and have similar degrees of filling [$F = 0.90\text{--}0.95$; $F = V_{\text{liquid}}/(V_{\text{liquid}} + V_{\text{vapour}})$; Shepherd *et al.*, 1985].

Four fluid-inclusion populations (Fig. 7), hereafter named FP1 to FP4, can be distinguished, based on their distribution in zoned quartz crystals.

FP1: primary inclusions (5 to 30 μm) form concentric arrays along growth surfaces, and are characterised by variable shapes (*i.e.*, elliptical, spherical, oblate, irregular, and rare negative crystals).

FP2: a second type of primary inclusions (10–50 μm) occurs either isolated or in small clusters, and

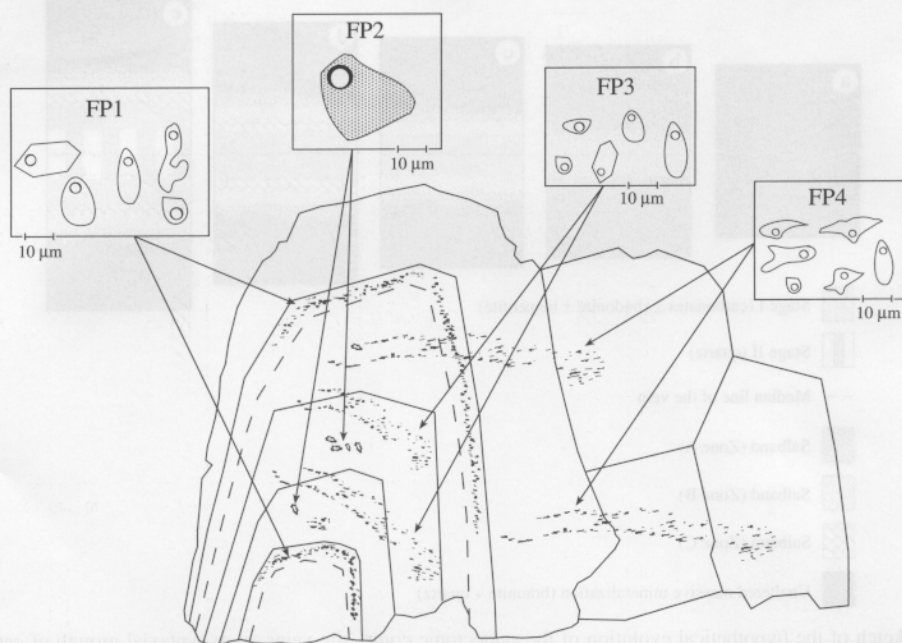


Fig. 7. Sketch of fluid-inclusion populations in zoned quartz: FP1, primary fluid inclusions along growth zones; FP2, isolated primary fluid inclusions; FP3, pseudosecondary fluid inclusions in intragranular trails; FP4, secondary fluid inclusions in intergranular trails. Within squares are depicted the most common morphologies of the fluid inclusions from the four recognised populations.

is commonly located between the growth zones of quartz crystals, particularly in the inner and intermediate growth domains. These inclusions differ from FP1, since they have larger sizes and, most important, they are characterised by a light-brownish cloudy appearance. Their shape is commonly oblate or spheroidal.

FP3: pseudosecondary fluid inclusions (5 to 30 μm) are present in short intragranular trails that end abruptly at growth-zone boundaries. These are very similar both in shape and dimensions to FP1 inclusions.

FP4: secondary fluid inclusions (5 to 20 μm) occur along trails cross-cutting growth zones and crystal boundaries, without any preferred orientation. These trails are clearly related to late healed microfractures. Inclusions are commonly decrepitated and characterised by very variable shapes. In some cases, secondary inclusions are so abundant as to give to the quartz crystals a milky appearance.

Results of fluid-inclusion studies

Microthermometry and SEM analyses were performed on all fluid-inclusion populations described above. Based on these results two main types of fluid compositions can be distinguished, hereafter named Fluid A and Fluid B. Raman microspectroscopy analyses were performed only in selected type B fluid inclusions.

Fluid A is characteristic for FP1, FP3, and FP4 fluid-inclusion populations. On cooling, all inclusions freeze instantaneously at temperatures (T_f) between -25 and -30°C . On subsequent heating, last ice-melting temperatures (TM_{ice}) are recorded between -1.1 and -0.1°C . The temperature of first melting (T_e) was never observed, probably because of very little melt produced at the eutectic point in these low-salinity fluid systems. Overall microthermometric behaviour indicates that the fluid inclusions FP1, FP3, and PF4 are all characterised by very low salinity NaCl-KCl-bearing fluids (max. salinity $\leq 1.5\%$ in NaCl eq. wt%; Fig. 8).

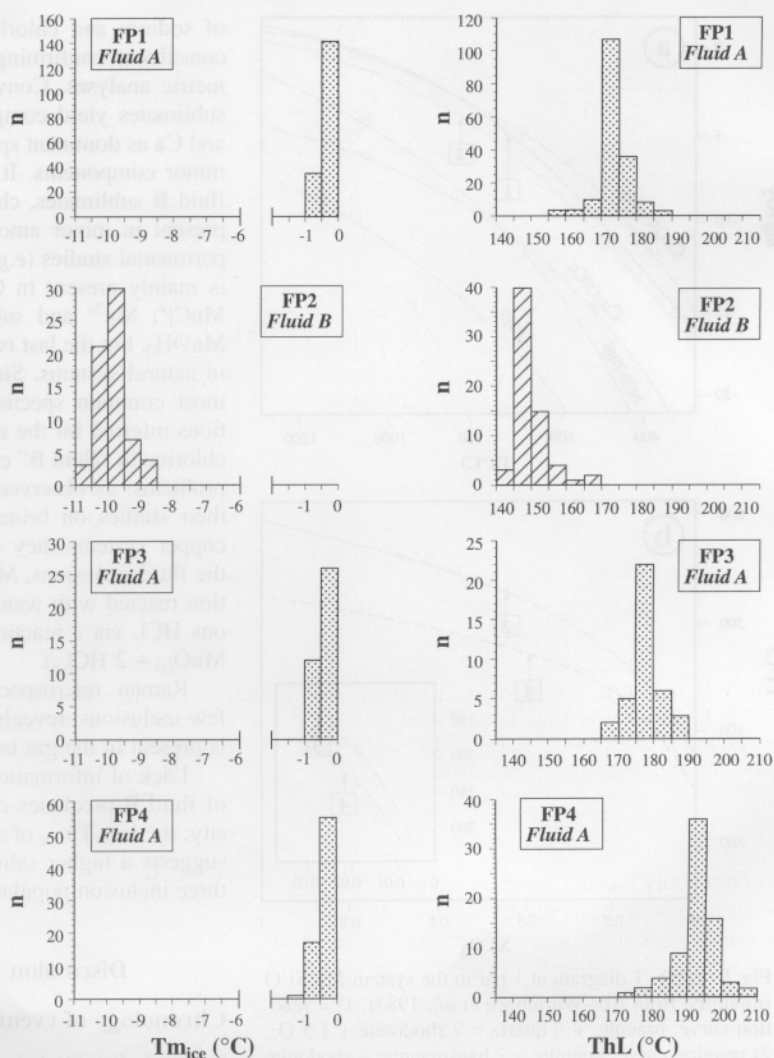


Fig. 8. Frequency histograms for final melting (T_{mice}) and homogenisation temperatures (ThL) in the different inclusion types.

Homogenisation temperatures [$Th(L+V) \rightarrow L$] are between 150 and 210°C; a temperature increase is observed from primary inclusions (FP1) to pseudosecondary and secondary inclusions (FP3 and FP4; Fig. 8). Relative densities (d), calculated with the Zhang & Frantz (1987) equation, slightly decrease from FP1 ($d = 0.93\text{--}0.89\text{ g/cm}^3$) to FP3 ($d = 0.91\text{--}0.88\text{ g/cm}^3$) and FP4 ($d = 0.90\text{--}0.86\text{ g/cm}^3$) (MacFlincor software; Brown & Hagemann, 1994).

Fluid B occurs only in FP2 fluid inclusions and shows a different microthermometric behaviour (Fig. 8). On cooling, all inclusions freeze at low temperatures ($-45^\circ\text{C} \leq T_f \leq -52^\circ\text{C}$) and form masses of brownish aggregates, which give a

speckled appearance to the inclusions. As the temperature rises, the inclusions take a very granular appearance, and a first liquid is observed at about -39°C (T_x). At this temperature, four phases co-exist; vapour, liquid, ice and fine-grained rounded brownish crystals. On further heating, the brownish solids progressively melt and disappear at $-22/\text{--}20^\circ\text{C}$. The temperature of the final melting of ice (T_{mice}) ranges between -8.6 and -10.5°C . All inclusions homogenise to the liquid ($L+V \rightarrow L$) and ThL 's from 135 to 165°C, with a frequency peak at 140/145°C.

The temperatures of the observed phase transitions indicate that type B fluid does not belong to the same chemical system as fluid A (*i.e.*, H_2O -

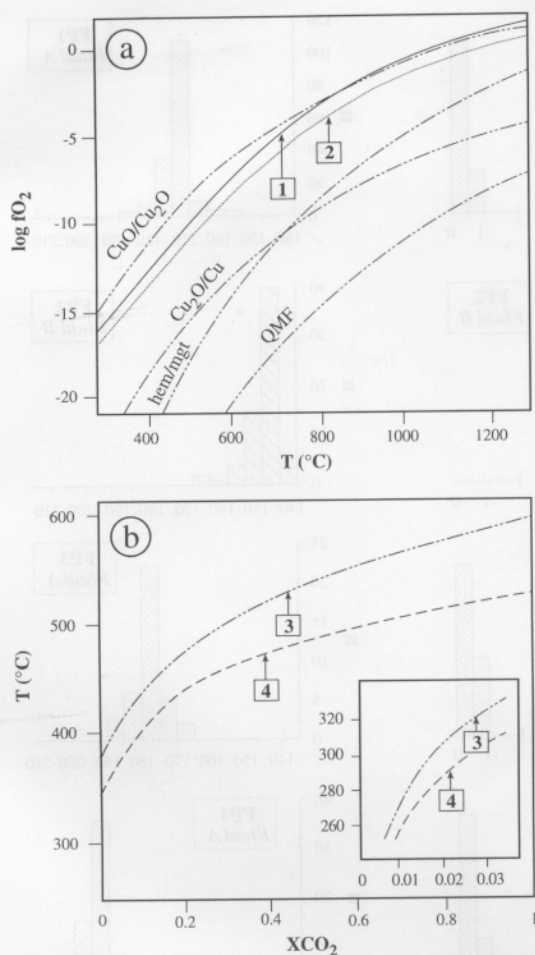


Fig. 9. a) $\log f_{O_2}$ -T diagram at 1 bar in the system Mn-Si-O (modified from Abs-Wurmbach *et al.*, 1983). 1) = reaction curve: braunite + 6 quartz = 7 rhodonite + 1.5 O₂. 2) reaction curve: braunite = 2 hausmannite + rhodonite + 0.5 O₂. b) T-XCO₂ diagram at 1 kbar for reaction 3): johannsenite + CO₂ = rhodonite + calcite + quartz, and 4): rhodonite + CO₂ = rhodochrosite + quartz (modified from Abrecht, 1985).

NaCl-KCl). Based on the very low temperature of freezing and, most importantly, on the depression of the temperatures of first melting, fluid B represents a complex solution system.

Because of the doubtful nature of the solutes present in fluid B, and in order to characterise its chemistry, SEM analyses were performed on open fluid inclusions from selected chips that were previously used for microthermometric analyses. Energy-dispersive X-ray (EDX) spectra of fluid A sublimates indicate that they are composed mostly

of sodium and chlorine, with calcium as minor constituent, confirming the results of microthermometric analyses. Conversely, analyses of fluid B sublimates yield complex EDX spectra with Mn and Ca as dominant species and Na, Fe and Mg as minor components. It is worth noting that in all fluid B sublimates, chlorine is lacking or is only present in minor amounts. As evidenced by experimental studies (*e.g.*, Bockor, 1985) manganese is mainly present in Cl-rich solutions as MnCl₂, MnCl⁺, Mn²⁺ and subordinately as MnOH and MnOH₂, but the last two species are very unlikely in natural systems. Since chlorides are by far the most common species at the P-T-Eh-pH conditions inferred for the study system, the absence of chlorine in "fluid B" could be related to analytical problems, as observed by Quan *et al.* (1987). In their studies on brine inclusions from porphyry copper systems they suggested that, on opening the fluid inclusions, Mn and Ca chlorides in solution reacted with water to form oxides and gaseous HCl, via a reaction type: $MnCl_{2(aq)} + H_2O = MnO_{(s)} + 2 HCl_{(g)}$.

Raman microspectroscopy, performed on a few inclusions, reveals that very-low-density CH₄ is present in the gas bubble, but no CO₂.

Lack of information on the exact composition of fluid B precludes calculation of the fluid density; the low T_{mice} of all FP2 inclusions indirectly suggests a higher salinity, compared to the other three inclusion populations.

Discussion and conclusions

Chronology of events

Textural characteristics of Mn ores from the Gambatesa District indicate that braunite early formed diagenetically at the expense of primary sedimentary low-crystallinity, high-valence Mn oxides and/or Mn hydroxides.

During Upper Cretaceous-Lower Cenozoic orogenic events layered manganese ore bodies underwent mobilisation and thickening in areas of intense deformation, resulting in the formation of massive lens-shaped ore bodies (MM) at fold hinges and boudin-like ore bodies (MB) along fold limbs. The braunite + quartz assemblage remained stable during the overall prograde (up to prehnite-pumpellyite-facies conditions) and subsequent retrograde and decompressive evolution.

At the hinges of mineralised mesoscopic chevron folds, the formation of complex fracture net-

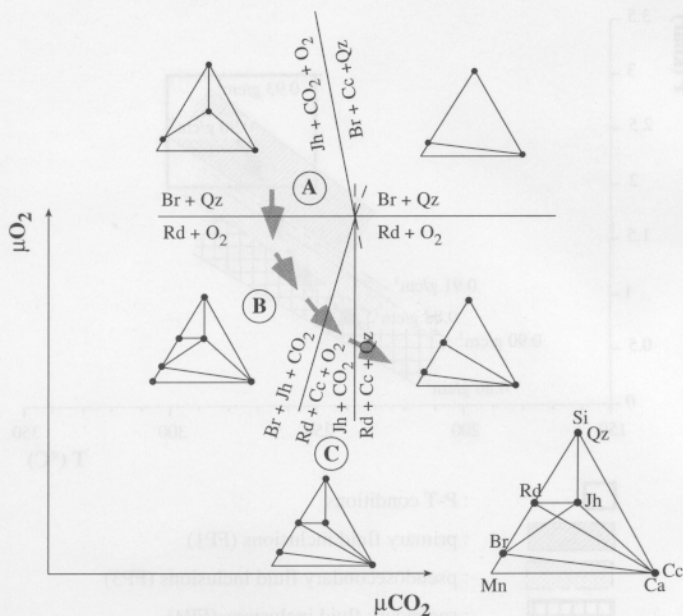


Fig. 10. Progressive fluid evolution according to the observed reactions in the isothermal, isobaric μCO_2 - μO_2 diagram for the system Mn^{2+} -Si-Ca-C-O₂ and for temperature below the johannsenite-bustamite equilibrium (redrawn from Cabella *et al.*, 1991). Reaction zones A), B), C) and abbreviations as in Fig. 5.

works provided pathways for local syntectonic and synmetamorphic fluid circulation. Interaction between metamorphic fluids and manganese ore triggered braunite breakdown to form hydrous Mn silicates, Mn carbonates and Mn carbonates.

The assemblage braunite + quartz in the unaltered massive mineralisations suggests initial f_{O_2} conditions along the $\text{MnO}_2/\text{Mn}_2\text{O}_3$ buffer, as calculated in the system Mn-Si-O between 3–7 kbar and 350–675°C (Abs-Wurmbach *et al.*, 1983). In the early stage of braunite + quartz alteration mineral equilibria indicate that fluid-rock interaction should have been triggered by an H_2O - CO_2 fluid at first with high water activity, and occurred under decreasing f_{O_2} , at least before braunite breakdown through the reaction braunite + quartz \rightarrow rhodonite (reaction II, Fig. 5 and reaction I, Fig. 9a). This reaction, along with the lack of hausmannite (Mn_3O_4) in all the observed assemblages, implies f_{O_2} conditions slightly below the $\text{CuO}/\text{Cu}_2\text{O}$ buffer (reaction 2, Fig. 9a; Abs-Wurmbach *et al.*, 1983).

Based on the progressive mineralogical reactions it is likely that during the successive evolution, the fluid-rock interaction caused water consumption with an indirect increase in the CO_2 content of the residual fluid which, at first, is responsible for the precipitation of Mn-bearing calcite along with rhodonite and, in the late stages, for the widespread precipitation of Mn-rich carbonates (rhodochrosite and "pseudokutnahorite")

both in reaction zones and in outer rims of the veins. As proposed by Peters *et al.* (1978), a progressive increase of X_{CO_2} in the fluid well agrees with the observed spatial and temporal variations in the carbonate types, and, above all, with the compositional variations of coexisting rhodonite and carbonate pairs (Fig. 3a, b; Table 1 and 2).

Following this hypothesis, in the early stage a very low X_{CO_2} value would be sufficient for a widespread carbonatisation of clinopyroxene (johannsenite). Albrecht (1985) illustrated that at low pressures and at temperatures below 350°C johannsenite breakdown takes place at X_{CO_2} values below 0.01 (reaction 3, Fig. 9b), and the reaction products are rhodonite and Mn-bearing calcite. As X_{CO_2} increases, part of the available manganese is partitioned into carbonates, allowing rhodochrosite formation both in the metasomatic alteration zones and in the veins as the last carbonate generation. Finally, johannsenite breakdown and massive carbonate precipitation presumably causes silica enrichment in the residual fluid, and consequently the late-stage precipitation of monomineralic quartz infillings in the central part of the vein (Fig. 6e).

The complete set of the observed reactions constrained in the isothermal-isobaric μO_2 - μCO_2 diagram, proposed by Cabella *et al.* (1991), illustrates the overall evolution discussed above (Fig. 10).

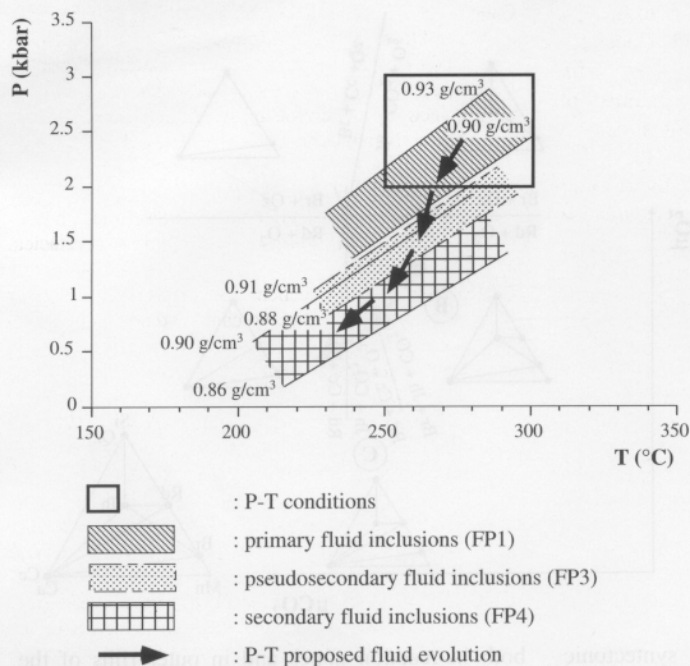


Fig. 11. P-T evolution of fluid circulation during the main tectono-metamorphic event. Isochores calculated with Zhang & Frantz (1987) equations; P-T box from Lucchetti *et al.* (1990).

P-T evolution and origin of fluids

Isochores calculated from the primary fluid-inclusion population (fluid A, FP1) are consistent with P-T conditions during peak regional metamorphism in the Gambatesa District (250–300 °C; 2–3 kbar; Lucchetti *et al.*, 1990). This suggests that the quartz infilling during the veining processes coincided with the main tectono-metamorphic event and took place most likely at peak conditions (Fig. 11). Starting from peak-metamorphic conditions, the isochore distribution of the pseudo-secondary and secondary fluid-inclusion populations (FP3 and FP4) points to an overall decompressive retrograde P-T evolution of the veins (Fig. 11).

The distribution of type B fluids trapped in fluid-inclusion population FP2 suggests that they represent relicts of a temporally defined episode of fluid-ore interaction, which occurred during the early stage of metamorphic veining and metasomatic alteration of the adjoining Mn ore.

Microthermometry, SEM, and Raman analyses indicate that fluid B is an H₂O-dominated fluid containing minor amounts of methane and carrying Mn, Ca, and minor Na, Mg and Fe in solution. Due to the large number of different cations involved, its actual salinity remains speculative. Our data indicate a fairly complex solution system with Mn²⁺ as the dominant cation, in good agree-

ment with the alteration of the wall rocks. Thus, fluid B documents the early interaction between fluids and massive Mn mineralization that caused the breakdown of braunite and saturated the fluids in Mn, Ca, Fe, Mg, and Si. Overall, there is no evidence for significant fluid migration between adjoining layers of ore and rock, during deformation and metamorphism. Mass transfer appears to have been restricted to a scale of at most several metres.

Fluid A may have triggered all secondary replacement reactions of the association braunite + quartz. The absence of CO₂ in type A fluid inclusions may be explained with the fact that an XCO₂ below 0.01 will never be detected in these microsystems with the available analytical techniques (*e.g.*, Raman microspectrometers have a detection limit in the range of two orders of magnitude higher, for these low-density gas bubbles; Burke, 1994). Thus, small amounts of CO₂ might be present in type A fluids and remain undetected.

It is envisaged that vein formation resulted from local processes, and fluids were drawn into opening cracks from the immediate vicinity. The present study indicates that fluids during the syn-tectonic evolution of Mn ores may be confined within individual layers, which in turns implies that the permeability of rocks at these low-metamorphic grades was already relatively low.

Acknowledgements: We are grateful to R. Cabella, L. Cortesogno, G. Giorgetti, G. Lucchetti, M. Scambelluri and F. Tecce for useful discussions of an earlier version of the manuscript. We further acknowledge S.M. Kars for assistance during SEM analyses, and E.A.J. Burke for Raman analyses. Thoughtful reviews by J. Gutzmer, P. Lattanzi and an anonymous reviewer improved considerably the manuscript.

References

- Abrecht, J. (1985): Manganiferous pyroxenes and pyroxenoids from three Pb-Zn-Cu skarn deposits. *Contrib. Mineral. Petrol.*, **89**, 379-393.
- Abs-Wurmbach, I. (1980): Miscibility and compatibility of braunite, $\text{Mn}^{2+}\text{Mn}_6^{3+}\text{O}_8\text{SiO}_4$ in the system Mn-Si-O at 1 atm. in air. *Contrib. Mineral. Petrol.*, **71**, 393-399.
- Abs-Wurmbach, I., Peters, Tj., Langer, K., Schreyer, W. (1983): Phase relations in the system Mn-Si-O: an experimental and petrological study. *N. Jb. Mineral. Abh.*, **146**, 158-279.
- Bhattacharyya, P.K., Dasgupta, S., Fukuoka, M., Roy, S. (1984): Geochemistry of braunite and associated phases in metamorphosed non-calcareous manganese ores of India. *Contrib. Mineral. Petrol.*, **87**, 65-71.
- Boctor, N.Z. (1985): Rhodonite solubility and thermodynamic properties of aqueous MnCl_2 in the system $\text{MnO-SiO}_2\text{-HCl-H}_2\text{O}$. *Geochim. Cosmochim. Acta*, **49**, 565-575.
- Bonatti, E., Zerbi, M., Kay, T., Rydell, H. (1976): Metaliferous deposits from the Apennine ophiolites: Mesozoic equivalents of modern deposits from oceanic spreading centers. *Geol. Soc. Am. Bull.*, **87**, 83-94.
- Brown, P.E. & Hagemann, S.G. (1994): MacFlinCor: a computer program for fluid inclusion data reduction and manipulation. in "Fluid inclusions in minerals: methods and applications", De Vivo, B. & Frezzotti, M.-L., eds., Blacksburg, Virginia Polytechnic Institute and State University Press, 231-250.
- Burke, E.A.J. (1994): Raman microspectrometry of fluid inclusions: the daily practice. in "Fluid inclusions in minerals: methods and applications", De Vivo, B. & Frezzotti, M.-L., eds., Blacksburg, Virginia Polytechnic Institute and State University Press, 25-44.
- Cabella, R., Cortesogno, L., Gaggero, L. (1994): Hydrothermal contributions to cherts deposition in Northern Apennines: a preliminary report. *Ophioliti*, **19**, 367-376.
- Cabella, R., Gaggero, L., Lucchetti, G. (1991): Isothermal-isobaric mineral equilibria in braunite-, rhodonite-, johannsenite-, calcite-bearing assemblages from Northern Apennine metacherts (Italy). *Lithos*, **27**, 149-154.
- Cabella, R., Lucchetti, G., Marescotti, P. (1998): Mn-ores from Eastern Liguria ophiolitic sequences ("Diaspri di Monte Alpe Formation" Northern Apennines, Italy). *Trends in Mineralogy*, **2**, 1-17.
- Capobianco, C. & Navrotsky, A. (1987): Solid-solution thermodynamics in $\text{CaCO}_3\text{-MnCO}_3$. *Am. Mineral.*, **72**, 312-318.
- Cortesogno, L., Galbiati, B., Principi, G. (1987): Note alla Carta geologica delle ophioliti del Bracco e ricostruzione della paleogeografia giurassico-cretacea. *Ophioliti*, **12**, 261-342.
- Cortesogno, L. & Lucchetti, G. (1984): Ocean floor metamorphism of the volcanic and sedimentary sequences in the Northern Apennine Ophiolites: mineralogical and paragenetic features. *Ophioliti*, **9**, 363-400.
- Cortesogno, L., Lucchetti, G., Penco, A.M. (1979): Le mineralizzazioni a manganese nei diaspri delle ophioliti liguri: mineralogia e genesi. *Rend. S.I.M.P.*, **35**, 151-197.
- Cox, S.F. (1987): Antitaxial crack-seal vein microstructures and their relationship to displacement paths. *J. Struct. Geol.*, **9** (7), 779-787.
- Cox, S.F. & Etheridge, M.A. (1983): Crack-seal fibre growth mechanisms and their significance in the development of oriented layer silicate structure. *Tectonophysics*, **92**, 147-170.
- Dasgupta, H.C. & Manickavasagam, R.M. (1981): Chemical and X-ray investigation of braunite from the metamorphosed manganiferous sediments of India. *N. Jb. Mineral. Abh.*, **142**, 149-160.
- Eggleton, R.A. & Guggenheim, S. (1994): The use of electron optical methods to determine the crystal structure of a modulated phyllosilicate: parsettenite. *Am. Mineral.*, **79**, 426-437.
- Goldsmith, J.R. & Graf, D. (1957): The system CaO-MnO-CO_2 : solid solution and decomposition relations. *Geochim. Cosmochim. Acta*, **11**, 310-334.
- Heinrich, A.R., Eggleton, R.A., Guggenheim, S. (1994): Structure and polytypism of bementite, a modulated layer silicate. *Am. Mineral.*, **79**, 91-106.
- Lucchetti, G., Cabella, R., Cortesogno, L. (1990): Pumpellyites and coexisting minerals in different low-grade metamorphic facies of Liguria, Italy. *J. Metam. Geol.*, **8**, 539-550.
- Marescotti, P. & Cabella, R. (1996): Significance of chemical variations in a chert sequence of the "Diaspri di M. Alpe Formation" (Val Graveglia, Northern Apennine, Italy). *Ophioliti*, **21**, 139-144.
- Ostwald, J. (1992): Mineralogy, paragenesis and genesis of the braunite deposits of the Mary Valley Manganese Belt, Queensland, Australia. *Mineral. Dep.*, **28** (1), 326-335.
- Peacor, D.R., Essene, E.J., Gaines, A.M. (1987): Petrologic and crystal-chemical implications of cation order-disorder in kutnahorite: $\text{CaMn}(\text{CO}_3)_2$. *Am. Mineral.*, **72**, 319-328.
- Peters, Tj., Trommsdorff, V., Sommerauer, J. (1978): Manganese pyroxenoids and carbonates: critical

- phase relations in metamorphic assemblages from the Alps. *Contrib. Mineral. Petrol.*, **66**, 383-388.
- Principi, G., Cortesogno, L., Cellai, D., Gaggero, L., Garuti, G., Gazzotti, M., Passerini, P., Treves, B. (1992): Le ofioliti dell'Appennino Settentrionale. *Atti Convegno SIMP*, Firenze 21-23/9/1992, Guida all'escursione, 1-76.
- Quan, R.A., Cloke, P.L., Kesler, S.E. (1987): Chemical analyses of halite trends inclusions from the Granisle Porphyry copper deposits, British Columbia. *Econ. Geol.*, **82**, 1912-1930.
- Ramsay, J.G. & Huber, M.I. (1983): The techniques of modern structural geology, volume 1: strain analysis. Academic Press, London: 305 p.
- Roy, S. (1980): Genesis of sedimentary manganese formations: processes and products in recent and older geological ages. in "Geology and geochemistry of manganese", Varentsov, M. & Grassely, G.Y., eds., Vol. 2, Akadémiai Kiadó, Budapest, 13-44.
- (1981): Manganese deposits. Academic Press, London, 458 p.
- Shepherd, T.J., Rankin, A.H., Alderton, D.H.M. (1985): A practical guide to fluid inclusion studies. Blackie & Son Ltd., Glasgow and London, 239 p.
- Urai, J.L., Williams, P.F., Van Roermund, H.L.M. (1991): Kinematics of crystal growth in syntectonic fibrous veins. *J. Struct. Geol.*, **13** (7), 823-836.
- Usui, A. & Someya, M. (1997): Distribution and composition of marine hydrogenetic and hydrothermal manganese deposits in northwest Pacific. in "Manganese mineralization: geochemistry and mineralogy of terrestrial and marine deposits". Nicholson, K., Hein, J.R., Bühn, B., Dasgupta, S., eds. Geol. Soc. Spec. Publ., London, **119**, 177-198.
- Zhang, Y. & Frantz, J.D. (1987): Determination of the homogenization temperatures and densities of supercritical fluids in the system NaCl-KCl-CaCl₂-H₂O using synthetic fluid inclusions. *Chemical Geol.*, **64**, 335-350.

Received 7 January 1999

Modified version received 27 July 1999

Accepted 2 November 1999